Spatial and temporal analyses using Terrestrial LiDAR for monitoring of landslides to determine key slope instability thresholds: Examples from Northern Ireland and Canada

Andrew D.F. Bell, Dr Jennifer M. McKinley
School of Geography, Archaeology and Palaeoecology, Queens University Belfast, BT7 1NN, Northern Ireland, UK
Dr David A.B. Hughes
School of Planning, Architecture and Civil Engineering, Queens University Belfast, BT7 1NN, Northern Ireland, UK
Dr Michael Hendry, Dr Renato Macciotta
Canadian Rail Research Laboratory (CaRRL), Natural Resources Engineering Faculty, University of Alberta, Edmonton, Alberta, Canada

ABSTRACT
Landslides in the form of debris flows, large scale rotational features, rockfalls and composite mudflows impact transport corridors cut off local communities and in some instances result in loss of life. This study presents collaborative research for complex spatial analysis landslide monitoring methods used for predicting and characterising landslide activity along transport corridors. Local scale ground monitoring approaches using Terrestrial LiDAR scanning (TLS) are employed for the monitoring of changes in selected slopes. Results are shown from on-going TLS monitoring of sites registered within a site specific geodectically referenced network. Results are presented illustrating temporal monitoring of landslides for two case study sites: 1. A coastal landslide impacting on a road transport corridor, Straidkilly Point, Glenarm, Co. Antrim, Northern Ireland and, 2. A rail transport cutting, Cascade Rockfall, Fraser River, BC, Canada. These studies demonstrate repeat monitoring and spatial morphological approaches using TLS enable characterisation and prediction of potential areas of slope stability issues. Spatial parameters, particularly measures of roughness, give indications of recent slope movements or accumulation of material. Slope angle, curvature and aspect maps provide indications of areas of potential instability.

RÉSUMÉ
Cette étude présente la recherche collaborative pour les méthodes de surveillance analyse spatiale des glissements de terrain complexes utilisées pour prédire et caractériser l'activité des glissements de terrain le long des corridors de transport. Local surveillance au sol à grande échelle des approches utilisant le balayage LiDAR terrestre (TLS) sont utilisés pour la surveillance des changements dans les pentes sélectionnés. Les résultats sont présentés de la surveillance continue TLS des sites enregistrés dans un site de réseau geodectically référence spécifique. Les résultats sont présentés illustrant le suivi temporel des glissements de terrain pour les sites d'étude de deux cas: 1. Un glissement de terrain côtier impact sur un corridor de transport routier , Straidkilly Point, Glenarm , comté d'Antrim, en Irlande du Nord et , 2. Une coupe de transport ferroviaire, Cascade chutes de pierres, du fleuve Fraser, en Colombie-Britannique, Canada. Ces études démontrent la surveillance de répétition et les approches morphologiques spatiales à l'aide TLS permettent la caractérisation et la prévision des domaines potentiels de problèmes de stabilité de la pente. Paramètres spatiaux, en particulier les mesures de rugosité , donnent des indications de mouvements de terrain récents ou accumulation de matières. Cartes angle de la pente, courbure et l'aspect fournissent des indications sur les zones d'instabilité potentielle.

1 INTRODUCTION

Landslides in the form of debris flows, large scale rotational features, rockfalls and composite mudflows impact transport corridors cut off local communities and in some instances result in loss of life. Recently technological advances in geomorphological studies of slopes using ground based Terrestrial LiDAR Scanning (TLS) has enabled slope stability issues to be effectively monitored and characterised (Oppikofer et al., 2009). TLS has been used in a number of studies including; structural monitoring of geomorphological units (Dunning et al. 2009; Nguyen et al. 2011), monitoring mass movements (Avian et al. 2009; Oppikofer et al., 2009; Baldo et al., 2009) and landslide characterisation (Jaboyedoff et al., 2009; Kasperski et al., 2010). The advantage of LiDAR is the generation of a high resolution Digital Terrain Model (DTM) enabling highly detailed classification of slope features and structural units (Ventura et al., 2011).

Multi-temporal DEMs have been used in a number of studies for the assessment of changes over time of landslides and slope failures (Mitasova et al. 2009; Dewitte et al. 2008; Prokop and Panholzer, 2009). Topographic change and analysis of DEMs resulting in DEMs of difference are an effective means for the determination of areas where the landscape is evolving or failing. Multi-temporal DTMs enable the characterisation of the landform and identification of changes in the

topography. The evolution of the hillslope can then be seen along with any distinct change in slope morphology. Monitoring using Terrestrial LiDAR demonstrates short scale temporal measurement of the responses and changes of the slope.

Previous work into the characterisation of landslide morphology using high resolution DTMs was initially carried out by McKean and Roering (2004), using roughness of the landslide as an indicator of previous movement patterns. Carvalli and Marchi (2008) supplement the analysis with detailed characterisation of landslide morphology using LiDAR sources. Glenn et al. (2006) characterize and differentiate landslide morphology and activity using multiple assessment methods. Trevisani et al. (2009) develop the characterisation of LiDAR coupled with variogram analysis for the characterisation of landslide activity.

Limitations of the current understanding identify a gap in the knowledge for a multi-temporal characterisation of slope morphological change. Characterisation and monitoring of slope stability issues with multiple spatial parameters leads to a better understanding of slope processes, with the added benefit of determining key slope instability thresholds. This is particularly advantageous when sites have limited access with the inability to install geotechnical measurement devices.

This research illustrates spatial and temporal analyses using Terrestrial LiDAR for monitoring of landslides to determine key slope instability thresholds. These thresholds are determined from temporal monitoring using TLS before predictive thresholds can be determined for these selected slopes. The temporal monitoring approach implements TLS for characterising the development of 2 Study areas: 1. observations for a composite flowslide in Co. Antrim, Northern Ireland and 2. rockfall site along the Fraser River, BC, Canada.

2 STUDY AREAS

2.1 Straidkilly Point

The Antrim Coast Road stretching from the seaport of Larne in the East to the famous Giant's Causeway in the North has a well-deserved reputation for being one of the most spectacular roads in Europe (Day, 2006). Despite this beauty, since construction in the 1830s there have been a number of locations along the road that have experienced instances of geotechnical instability, including rock falls at Garron Point and mudflows at Minnis North (Hutchinson et al. 1974). This paper examines a small (6000m^2) active flowslide at Straidkilly Point, North of Glenarm Village, on the A2 coastal road. More recently Straidkilly Point has experienced increased instance of instability, which has resulted in large volumes of debris being deposited on the A2 Coast Road, forcing road closures. Figure 1 illustrates one such failure event on 25th January 2010. Figure 2 illustrates the Leica HDS300 Scanstation on site during a monitoring period, with Table 1 detailing data and scan statistics.

Figure 1. Landslide debris at Straidkilly on A2 Coast Road

Figure 2. Leica Terrestrial LiDAR scanning of Stradkilly Point, Northern Ireland.

2.2 Cascade Rockfall

The study area at Cascade M3 (Cascade Mile 3) is a representative site of the Cascade subdivision located along the Fraser River valley, Southern British Columbia, Canada (Figure 3). 'Rockfall is one of the most significant geohazards encountered by railways along the Canadian Rockies' (Lan et al., 2010:213). Previous assessments in the area discuss methodologies for the application of LiDAR for spatial modeling approaches for hazard assessment (Lan et al., 2010). Rockfalls are frequent, having had an impact on the railway since construction, with records of the location of rockfalls dating back to the 1940s. The study area is dominated by intrusive rocks of quartz diorite and granodiorite with geotechnical conditions such as the lithology, weathering of bedrock, joint spacing/orientation and groundwater infiltration influencing the triggering of rockfall events (Wieczorek et al., 2008; Lan et al., 2010). The highest rockfall frequency is in February, corresponding to the highest number of freeze thaw cycles. Table 2 illustrates the date and

preliminary statistics for the Terrestrial LiDAR scanning at Cascade M3.

Figure 3. Cascade Rockfall site viewed from across the Fraser River from TLS scanning location

Table 1. Straidkilly Point, Scan dates, number and Average point density (pts/m^2) from Terrestrial LiDAR scanning

Scan Date	Scan Number	Code	Average Point Density (pts/m^2)
August 2011	1	STR1	1042.36
September 2011	2	STR2	858.31
October 2011	3	STR3	1326.20
January 2012	4	STR4	656.25
March 2012	5	STR5	837.26
May 2012	6	STR6	947.32
June 2012	7	STR7	1043.60
September 2012	8	STR8	1015.09
November 2012	9	STR9	1059.74
February 2013	10	STR10	701.12

Table 2. Cascade, Scan dates, number and Average point density (pts/m^2) from Terrestrial LiDAR scanning

Scan Date	Scan Number	Code	Average Point Density (pts/m^2)
August 2011	1	CAS1	52.59
October 2012	2	CAS2	50.31

3 METHODS

3.1 Terrestrial LiDAR Scanning

For Straidkilly study is based on a series of ten Terrestrial LiDAR Data acquisitions over an 18 month period (August 2011 to February 2013). The LiDAR data were acquired from a Leica Terrestrial LiDAR Scanner, HDS3000 Scan Station. Field operations were carried out on approximately a six weekly basis, weather permitting. Two different scan positions were used and registered with targets placed in the field. Georeferencing and positioning were achieved by a site-specific geodetic network of survey nails. Total Station surveying of the targets and survey nails into the site-specific network was carried out. Subsequent georeferencing from dGPS data was undertaken after scan registration. This enabled all scans to be within the same co-ordinate system, essential when analyzing temporal changes between the scans. Scan registration errors were all less than 6mm, within the tolerance of the LiDAR scanner. Survey nails were placed on stable surfaces outside of the slope.

Cascade is based on two TLS data acquisitions with the LiDAR data acquired from the Optech ILRIS-3D scanner. Slightly different georeferencing and position of the Optech derived point clouds mean manual post processing of the data for common points to process the data into the same coordinate system.

3.2 DTM analysis and slope morphological characterization

Once the Terrestrial LiDAR data was registered and post processed the raw LiDAR data were imported into *Lastools* (2013) for removal of above ground objects. Lastools is a powerful set of LiDAR analysis tools. Multiple tools are available for batch scriptable, multicore command line processing of LiDAR data. Tools are available in standalone modules or ArcGIS (ESRI, 2012) toolbox extension. Within the suite of Lastools, *lasground.exe* is a tool for bare earth extraction.

Following extraction of above ground objects, Post processed LiDAR point cloud data were imported into ArcGIS. Inverse distance weighting (IDW) with 32 neighbors and a power of 2, was used as the interpolation approach for the generation of the Digital Terrain Model (DTM), with cell size 0.05m for Straidkilly and 0.2m for Cascade. Multi-temporal DTMs are used to understand how a landform or feature of the landscape evolves over time (Avian et al., 2009; Corsini et al., 2009; Ventura et al. 2011). For the purposes of this study, generated DTMs for each survey period were analysed for changes in elevation relating to morphological changes in the structure of the slope. Characterisation of the temporal change in the DTMs is achieved by changes in elevation, the previous DTM being subtracted from the most recent. These are known as DTMs of Difference (DODs) and are generated using the raster calculator in ArcGIS. Temporal changes in elevation maps are generated characterising any movement in the main slope kinematic units. Areas exhibiting a negative change in the elevation are areas of depletion, with a positive change indicating areas of accumulation.

This study implements GRASS GIS (GRASS Development Team, 2012) for the spatio-morphological roughness assessment of slopes. *r.param.scale* and *r.neighbors* commands are used for generation of the standard deviation of slope angle (SD_{Slope}) as the slope roughness parameter. SD_{Slope} has been used in studies

for topographic roughness studies (Frankel and Dolan, 2007; Grohmann et al., 2011) for characterisation of landform morphology, with particular benefits including allowing for highly variable nature of studies. In addition to roughness parameters, morphological maps of slope angle are generated.

The landslide at Straidkilly is divided into 'Sectors' with delineation on the basis of areas exhibiting largest changes. Within these sectors specific 'zones' are characterised on the basis of morphological features and responses of the DODs over the TLS monitoring period. The analysis was carried out defining 2 broad sectors, A and B, with 3 Zones (I to VI) within each, representative of the terrain evolution over the monitoring period. Sectors spatially cover the main morphologic and structural zones of the landslide (Figure 5).

4 RESULTS AND DISCUSSION

4.1 Straidkilly

The evolution of the slope at Straidkilly is presented as Figure 4, illustrating the cumulative changes in elevation over the monitoring period. Changes in the elevation of the temporal DTMs show distinct changes in slope morphology. There is a propagation of the material processes on the slope. Failures occur and can be progressively mapped downlsope with the source area further up the slope clearly evident. Further losses of material result in the accumulation downslope can be tracked to originate from the top of the slope in a number of areas. A large area of accumulation can be seen at the base of the slope. There is a spatial variation in the main units of failure and areas of terrain evolution.

Figure 6&7 depict the spatial distribtuion of changes in slope angle over the monitoring period with Sector A, Zone I (Figure 6a), experiences limited changes until STR4, illustrated by a distinct peak at lower slope angles. Subsequent density of slope angles follow this with further peaks evident at lower slope angles, ~30^{o} to ~40^{o}, at STR5 and STR6. Similar response is found for Sector B, Zone IV (Figure 6d) with a wider base, suggesting larger spread of values, at STR1 and STR2, following decreases in density of higher slope angles, a response to depletion of material. This suggests there has been a distinct drop in higher slope angles occurring as a result of slope deformation (consolidation).

Mid slope Zones II & V display similar characteristics in response of slope angle to deformation of the slope. Development of the slope involves a lessening density of the higher slope angles, a narrowing of the curve representing lower mean slope angles and lower dispersion of values after movement. This is reiterated by a lessening in mean slope angle and lower standard deviation of values. Highest density for Zone V, is located at STR6 for ~30^{o}. Lowering densities of higher slope angles diminish over the monitoring period. Zone V provides an example of the pattern of density of slope angle towards consolidation of lower slope angles; starting of high, deformation occurs, finishing off lower.

Limited variation occurs at the foot of the slope with a move towards a Gausian distribution (Figure 6c). Interestingly, slight increases of higher slope angles occur as a result of formation of new breaks of slope, increases slope angels, of the accumulation material. This effect is clearly shown in Figure 6(f) with a lessening of lower slope angles (0-20^{o}) after STR2 and middle slope angles (~40-50^{o}) after STR3, in response to slope movements. A larger density of higher slope angles (>~60^{o}) occur after STR3, signifying the effect of the accumulation occurring at the foot of the flowslide during this scanning epoch.

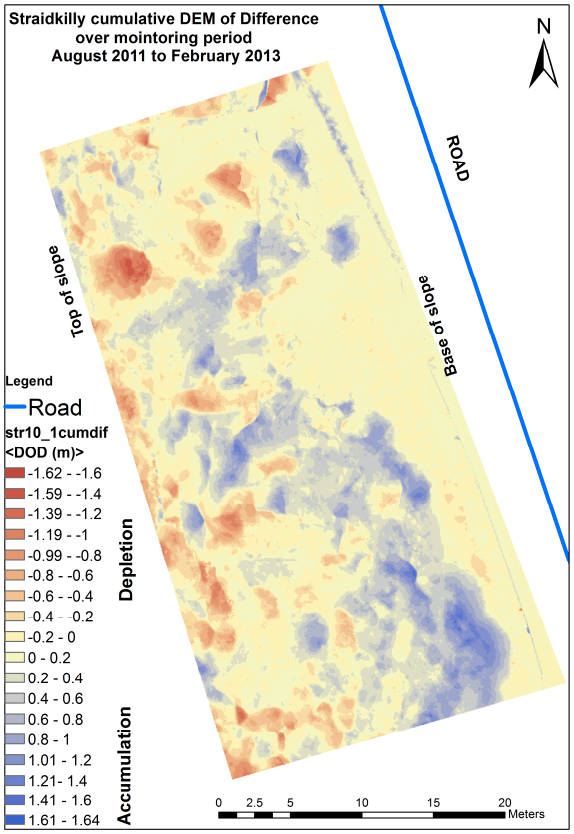

Figure 4. Straidkilly Point cumulative DTM of Difference of slope from temporal TLS monitoring August 2011 to February 2013. Sector A & B Zones I to IV for reference.

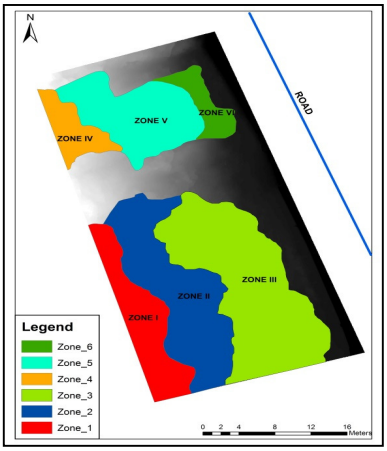

Figure 5. Colour coded representation of Zone deliamination for Straidkilly morphological areas for characterisation of temporal changes in slope parameters

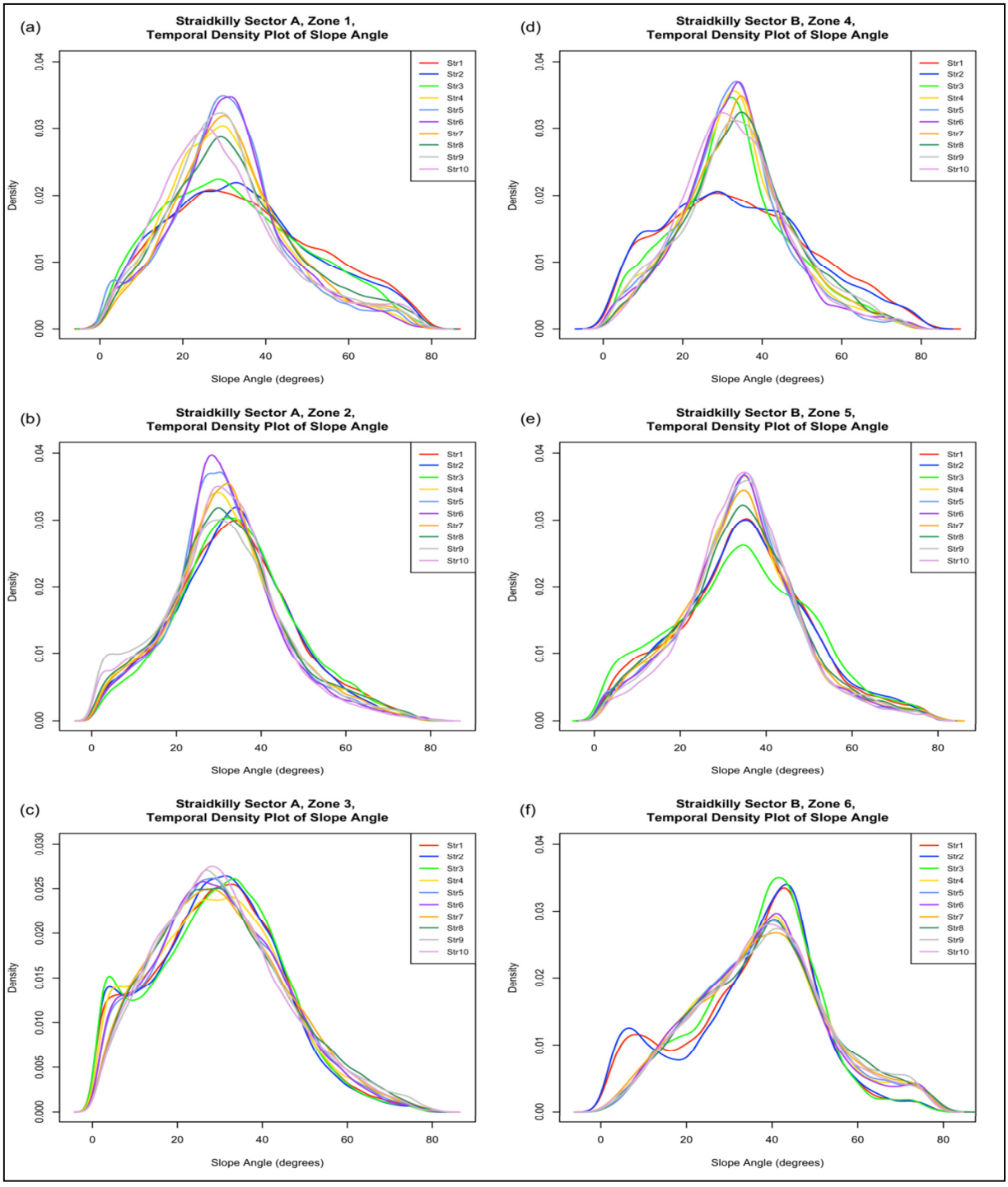

Figure 6: Density curves characterising development of slope angle over TLS monitoring period; Sector A (a) Zone I, (b) Zone II, (c)Zone III and Sector B (d) Zone IV, (e) Zone V and (f) Zone VI

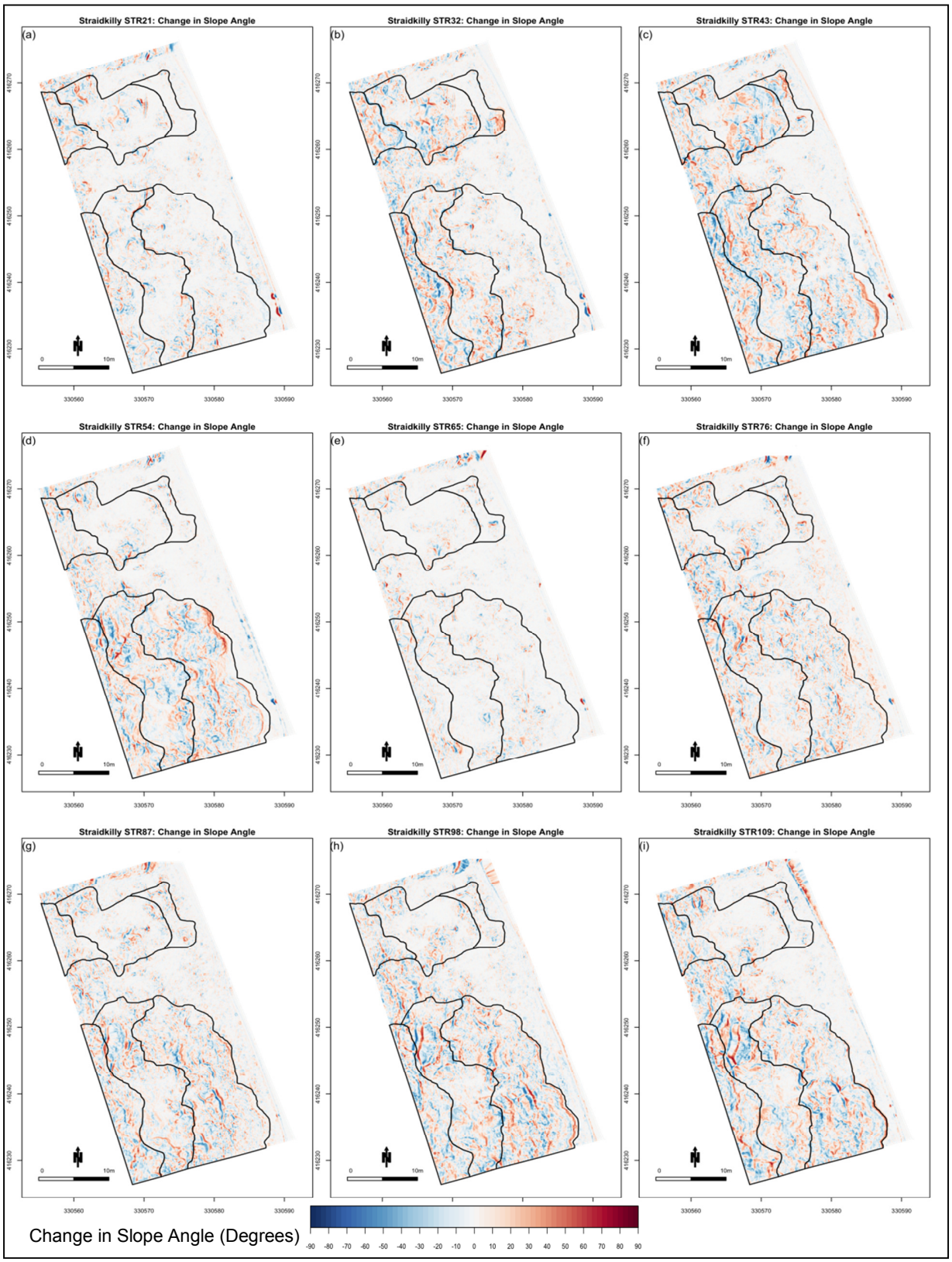

Figure 7: Spatial distribution of temporal changes in slope angle STR1 to STR10, Sector A & B, Zones I – VI for reference. Blue = decreases in slope angle, red = increases in slope angle

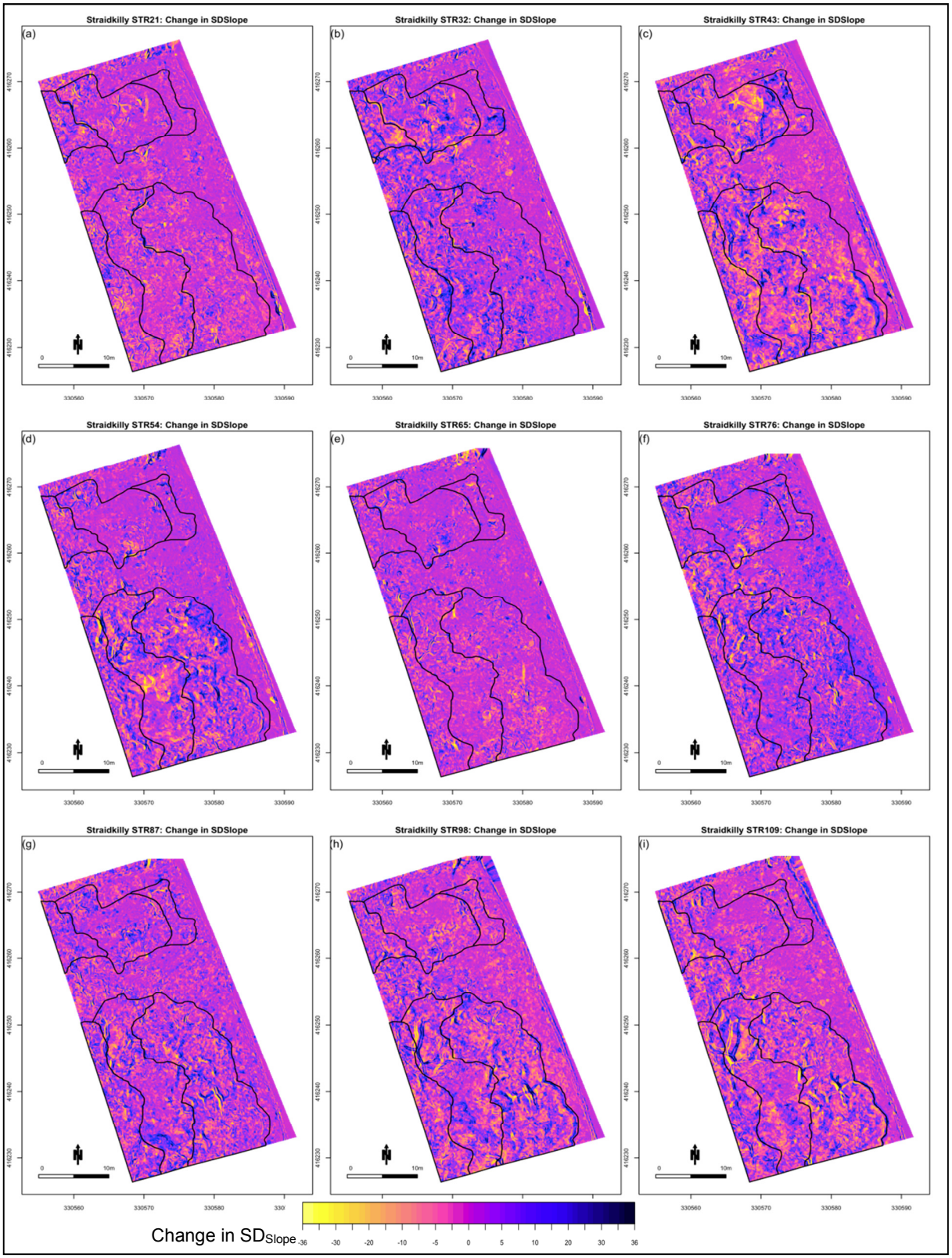

Figure 8(a-i). Temporal spatial distribution of changes in SD_{Slope} for Straidkilly TLS monitoring. Morphology Zones I to VI provided for reference

Figure 8(a-i), depicts the spatial distribution of SD_{Slope} over the TLS monitoring period. SD_{Slope} displays decreased roughness as a result of failure of minor scarps located at the top of the slope at STR21 and STR32, Zone I (Figure 8a&b). Increased roughness (red hue), is apparent further down the slope for STR32, Zone II (Figure 8b). STR43 displays an interesting pattern with green hues indicating decreases in roughness in responses to depletion of material. This spatial distribution impacts in Zone II with increased SD_{Slope} associated with accumulation of material. Accumulation at the foot of the flowslide is typified by distinct increases in roughness. Large deviations are present for SD_{Slope} at STR54 (Figure 8d) illustrating distinct spatial pattern of decreased roughness for Zone II which can be linked with increased roughness, due to accumulation of material, at the base of the slope in Zone III.

Further spectral responses are evident in Sector B, Zone IV to VI, STR32 to STR 43 (Figure 8a-c). Complex patterns of decreased SD_{Slope} are evident for Zone IV, indicating the depletion of material, with increased SD_{Slope} apparent in Zone V. Further developments in relation to the spatial characteristics are identified by decreases in Zone V with further failures, leaving smoother terrain behind, with increased roughness at Zone VI at the base of the slope. Zone II increases are present in two phases for STR32 and STR43 respectively indicating the effectiveness of the SD_{Slope} in characterising areas of increased roughness. Further evidence of SD_{Slope} response to slope deformation is illustrated in Sector A; STR87, STR98 and STR109 with decreases in SD_{Slope} characterised by increased further downslope in Zone III.

4.2 Cascade

The DTM of Difference for Cascade (Figure 9) highlights a large proportion of the slope as having undergone movement over the period between scans. Main areas of change are located at the head of the slope. A distinct debris flow channel is located where the main changes are occurring. Significant accumulation occurs on the main body of the slope adjacent to the rail line. Whilst further accumulation occurring at the toe of the slope, below the level of the rail line.

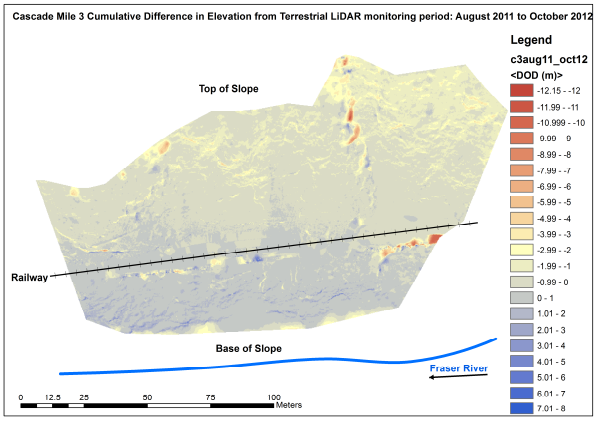

Figure 9. DTM of Difference for Cascade Rockfall from August 2011 to October 2012

Figure 10 illustrates significant increases in slope angle as a result of failure, due to formation of new rock scarps on site. The spatial distribution of changes in slope angle are extracted from the black polygon located in Figure 10 for the area undergoing the most significant movement. Reductions in density of higher slope angles is apparent from August 2011 to October 2012 (Figure 11). With a higher proportion of lower slope angles in October 2012 highlighting changes in structure of the slope. SD_{Slope} (Figure 12) displays a similar density distribution, with reduction in roughness post failure. This validates the findings in Section 4.1 for responses of the spatial parameters as a result of slope failures at Cascade.

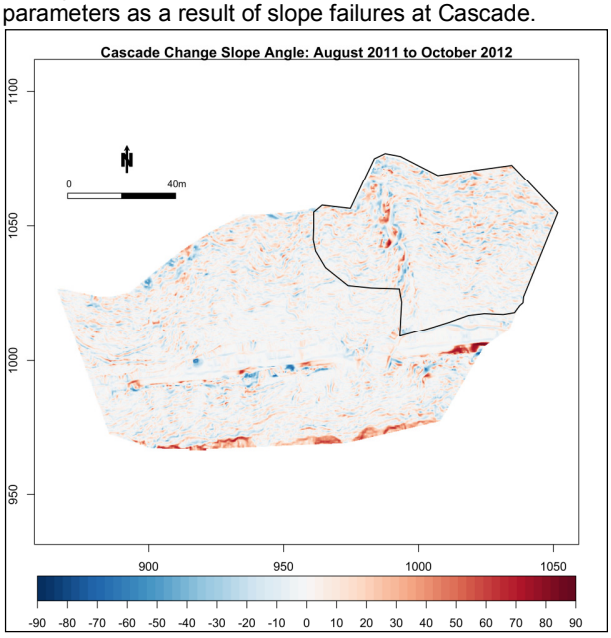

Figure 10. Spatial distribution of temporal changes in slope angle Cascade August 2011 to October 2012. Black box denotes zones for density curve extraction (Figure 11). Blue = decreases in slope angle, red = increases in slope angle.

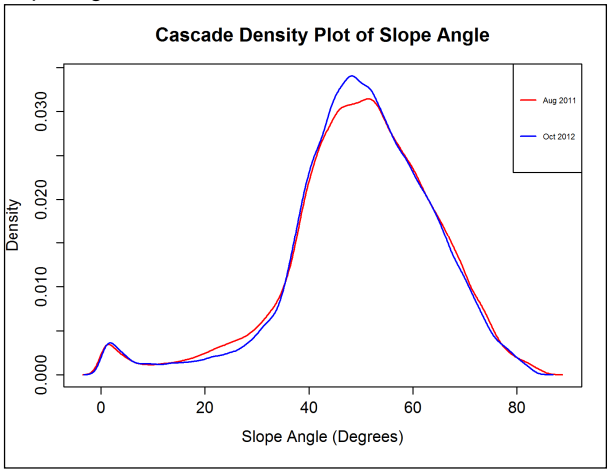

Figure 11. Density curve of spatial distribution of slope angle for Cascade from TLS August 2011 to October 2012

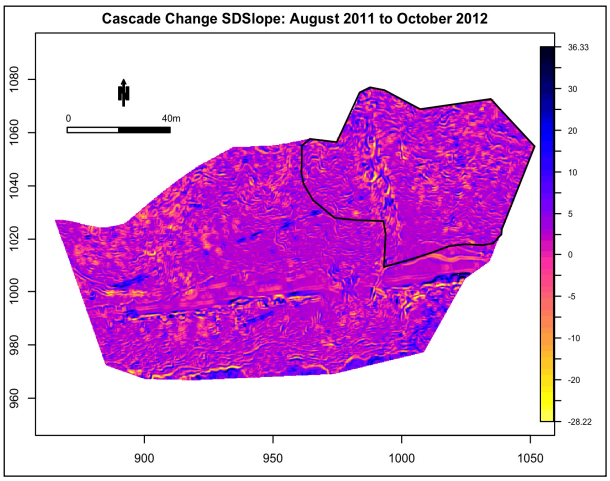

Figure 12. Cascade change in SD_{Slope} from August 2011 to October 2012

5 CONCLUSIONS

Terrestrial LiDAR has successful been applied for the monitoring of Straidkilly Point and Cascade rockfall in Canada. A number of conclusions can be drawn from this study:

- Spatial analysis approaches to the monitoring of the slope allow morphological change to be characterised with DTMs of difference, illustrating the main areas of depletion and accumulation between scans.
- The progressive failing nature of the flowslide is effectively characterized by TLS monitoring of the slope morphological parameters, primarily slope angle and roughness (SD_{Slope}). Characterisation of slope morphology provides insight into morphological parameterisation of slope movements with depiction of pre and post failure conditions of the slope morphology. Thus, providing indication of the key slope instability thresholds from these selected slopes.
- These studies demonstrate repeat monitoring and spatial morphological approaches using TLS enable characterisation and prediction of potential areas of slope stability issues. Failing slopes require monitoring for predictive thresholds to be determined. This in turn facilitates a multi-hazard interaction for the study areas with the development of a quasi-empirical model of failure from characterisation of the spatial parameters from the TLS.

ACKNOWLEDGEMENTS

The authors would like to thank the Department of Employment and Learning Northern Ireland, Roads Service NI and Canadian Rail Research Laboratory at the University of Alberta, Edmonton, Canada for their support and funding of this research.

REFERENCES

Avian, M., Kellerer-Pirklbauer, A and Bauer, A. 2009. LiDAR for monitoring mass Movements in permafrost environments at the cirque Hintres Langtal, Austria, between 2000 and 2008, Natural Hazards and Earth System Sciences, 9, 1087-1094

Baldo, M., Bicocchi, C., Chicchini, U., Giordan, D. and Lollino, G. 2009. LIDAR Monitoring of mass wasting processes: The Radicofani landslide, Province of Siena, Central Italy, Geomorphology, 105: 193-201

Bull, J.M., Miller, H., Gravely, D.M., Costello, D., Hikuroa, D.C.H. and Dix, J.K. 2010. Assessing debris flows using LiDAR differencing: 18th May 2005 Matata event, New Zealand, Geomorphology, 124: 75-84

Carvalli, M. and Marchi, L., 2008. Characterisation of the surface morphology of an alpine alluvial fan using airborne LiDAR, Natural Hazards and Earth System Sciences, 8, 323-333

Corsini, A., Borgatti, L., Caputo, G., De Simone, N., Sartini, G. and Truffelli, G. 2006. Investigation and monitoring in support of the structural mitigation of large slow moving landslidesL an example from Ca'Lita (Northern Apennines, Regiio Emilia, Italy), Natural Hazards and Earth System Sciences, 6: 55-61

Corsini, A., Borgatti, L., Cervi, F., Dahne, A., Ronchetti, F. and Sterzai, P. 2009. Estimating mass-wasting processes in active earth slides – earth flows with time series of High-resolution DEMS from photgrammetry and airborne LiDAR, Natural Hazards and Earth System Sciences, 9: 433-439

Dewitte, O., Jasselette, J.-C., Cornet, Y., Van Der Eeckhaut, M., Collignon, A., Poesen, J., and Demoulin, A. 2008. Tracking landslide displacements by multi-temporal DTMs: A combined aerial stereo photogrammetric and LiDAR approach in western Belgium, Engineering Geology, 99: 11-22

Day, C. 2006. *Ireland*. 6th ed. London: Cadogan Guides. p375.

Dunning, S.A., Massey, C.J. and Rosser, N.J. 2009. Structural and geomorphological features of landslides in the Bhutan Himalaya derived from Terrestrial Laser Scanning, Geomorphology, 103: 17-29

ESRI 2010. ArcGIS Desktop: Version 10, Environmental Systems Research Institute Redlands, CA.

Frankel, K.L, Dolan, J.F. 2007. Characterizing arid region alluvial fan surface roughness with airborne laser swath mapping digital topographic data, Journal of Geophysical Research: Earth Surface, 112 (F2)

Glenn, N.F., Streuker, D.R., Chadwick, D.J., Tackray, G.D. and Dorsch, S.J. 2006. Analysis of LiDAR-derived topographic information for the characterizing and differentiating landslide morphology and activity, Geomorphology 73: 131-148

GRASS Development Team. 2012. Geographic Resources Analysis Support System (GRASS), Software, Version 6.4.2. Open Source Geospatial Foundation. http://grass.osgeo.org

Grohmann, C.H., Smith, M.J., and Riccomini, C. 2011. Multiscale Analysis of Topographic Surface Roughness in the Midland Valley, Scotland, *IEEE*

Transaction on Geoscience and Remote Sensing, 49(4): 1200-1213

Hutchinson, J.N., Prior, D.B. and Stephens, N. 1974. Potentially dangerous surges in an Antrim mudslide Quarterly Journal of Engineering Geology, vol. 7: 363-376

Kasperski, J., Delacourt, C., Allemand, P., Potherat, P., Jaud, M. and Varrel, E. 2010. Application of Terrestrial Laser Scanner (TLS) to the study of the Sechilienne Landslide, (Isere, France), Remote Sensing, 2: 2785-2802

Jaboyedoff, M., Demers, D., Locat, J., Locat, A., Locat, P., Oppikoffer, T., Robitaille, D. and Turmel, D. 2009. Use of terrestrial laser scanning for the characterization of retrogressive landslides in sensitive clay and rotational landslides in river banks, Canadian Geotechnical Journal, 46: 1379-1390

Lastools. 2013. Lastools suite of LiDAR processing tools, Open source license, Martin Isenberg, http://rapidlasso.com/lastools/, Last Accessed: 26th April 2013

Lan, H., Martin, C.D., Zhou, C., and Lim, C.H. 2010. Rockfall hazard analysis using LiDAR and spatial modeling, *Geomorphology,* 118 (1-2): 213-223

McKean, J. and Roering, J. 2004. Objective landslide detection and surface morphology mapping using high-resolution airborne laser altimetry. Geomorphology, 57: 331-351

Mitasova,H., Overton, M.F., Recalde, J.J., Bernstein, D.J., and Freeman, C.W. 2009. Raster-Based Analysis of Coastal Terrain Dynamics from Multitemporal Lidar Data. Journal of Coastal Research, 25 (2): 507 – 514.

Nguyen, H.T., Fernandez-Steeger, T.M., Wiatr, T., Rodrigues, D. and Azzam, R. 2011. Use of terrestrial laser scanning for engineering geological applications on volcanic rock slopes – an example from Maderia island (Portugal), Natural Hazards and Earth System Sciences, 11: 807-817

Oppikofer, T., Jaboyedoff, M., Blikra, L., Derron, M-H. and Metzger, R. 2009. Characterization and monitoring of the Aknes rockslide using terrestrial lidar scanning, Natural Hazards and Earth System Sciences, 9: 1003-1019

Prokop, A., and Panholzer, H. 2009. Assessing the capability of terrestrial laser scanning for monitoring slow moving landslides, Natural Hazards and Earth System Sciences, 9: 1921-1928

Scheidl, C., Rickenmann, D. and Chiari, M. 2008. The use of airborne LiDAR data for the analysis of debris flow events in Switzerland, Natural Hazards and Earth System Sciences, 8: 1113-1127

Trevasani, S., Cavalli, M. and Marchi, L. 2009. Variogram maps from LiDAR data as fingerprints of surface morphology on scree slopes, Natural Hazards and Earth System Sciences, 9: 129-133

Ventura, G., Vilardo, G., Terranova, C. and Sessa, E. B. 2011. Tracking and evolution of complex active landslides by mutli-temporal airborne LiDAR data: The Montaguto landslide (Southern Italy), Remote Sensing of the Environment, 115, 3237-3248

Wieczorek, G.F., Stock, G.M., Reichenbach, P., Snyder, J.B., Borchers, J.W., and Godt, J.W. 2008. Investigation and hazard assessment of the 2003 and 2007 Staircase Falls rock falls, Yosemite National Park, California, USA, *Natural Hazards and Earth System Sciences, 8 (3): 421-432*